

# Learning a compass spin model with neural network quantum states

Eric Zou, Erik Long, and Erhai Zhao

*Department of Physics and Astronomy, George Mason University, Fairfax, Virginia 22030, USA*

Neural network quantum states provide a novel representation of the many-body states of interacting quantum systems and open up a promising route to solve frustrated quantum spin models that evade other numerical approaches. Yet its capacity to describe complex magnetic orders with large unit cells has not been demonstrated, and its performance in a rugged energy landscape has been questioned. Here we apply restricted Boltzmann machines and stochastic gradient descent to seek the ground states of a compass spin model on the honeycomb lattice, which unifies the Kitaev model, Ising model and the quantum  $120^\circ$  model with a single tuning parameter. We report calculation results on the variational energy, order parameters and correlation functions. The phase diagram obtained is in good agreement with the predictions of tensor network ansatz, demonstrating the capacity of restricted Boltzmann machines in learning the ground states of frustrated quantum spin Hamiltonians. The limitations of the calculation are discussed. A few strategies are outlined to address some of the challenges in machine learning frustrated quantum magnets.

## I. INTRODUCTION

Finding the ground-state wave functions of frustrated quantum spin models [1, 2] in two dimensions (2D) remains an outstanding theoretical challenge despite the great strides made in recent decades in the field of numerical many-body algorithms [3]. On the one hand, exact diagonalization and density matrix renormalization group, when applied to 2D, are restricted by the finite system size. On the other hand, variational Monte Carlo approaches, while being unbiased and valid in the thermodynamic limit, depend on the quality of the trial wave functions and tend to lose its prediction power due to the lack of convergence associated with the prevalent “negative sign problem” in frustrated quantum spin systems. Another efficient variational ansatz for quantum spin models is based on the tensor network (TN) representation of the many-body wave functions [4, 5]. One type of tensor networks known as projected entangled pair states, which generalize the matrix product states from one dimension to two dimensions, have been particularly successful when applied to quantum spin models [6]. The accuracy of TN ansatz however depends on the approximations employed when truncating and contracting the tensors. Given that each method has its advantages as well as drawbacks, a holistic approach will benefit from new numerical methods that can shed fresh light on this persistent problem.

Inspired by its tremendous success in machine learning and artificial intelligence [7], neural networks were recently proposed to solve quantum spin models [9, 10]. A generic wave function of  $N$  interacting spins, say  $S = 1/2$ , is a superposition of  $2^N$  basis states with complex coefficients. Mathematically, the wave function  $\psi(\mathbf{s})$  defines a mapping from vector  $\mathbf{s} = (s_1, s_2, \dots, s_N)$ , where  $s_i = \uparrow$  or  $\downarrow$ , to a complex number. Therefore, it can be thought of as a machine that gobbles up  $\mathbf{s}$  and spits out a complex number. While a rigorous proof is still lacking, it is conjectured that such mapping can be represented accurately by a sufficiently sophisticated neural network,

e.g. one with enough number of nodes, layers, and connections [8]. Then, to find the ground state of a given interacting spin Hamiltonian, all one needs to do is to train the network by adjusting its parameters stochastically so that the energy expectation value is minimized. This approach was pioneered by Carleo and Troyer, who represented the many-spin wave function as restricted Boltzmann machines (RBMs) and successfully applied it to solve the Heisenberg model on the square lattice [9]. In addition to RBM, the wave function can also be expressed as feed-forward neural networks or other neural network architectures. For example, Choo et al employed convolutional feed-forward neural networks to solve the  $J_1$ - $J_2$  model, a canonical example of frustrated magnets believed to host a quantum spin liquid, and obtained excellent energetics comparable to exact diagonalization and DMRG [11]. The  $J_1$ - $J_2$  model has also been investigated in Refs. [12–16] using the neural network ansatz. In a broader context, recent work has revealed a remarkable connection between the neural-network and the tensor-network representation of quantum many-body states despite their differences in appearance and origin [17–19]. It was shown that neural network quantum states can describe states with topological order, even with entanglement entropy beyond the area law [20–22]. Beyond quantum spin models, neural network quantum states have been also applied to strongly correlated fermions [23–25].

These promising developments have raised many open questions. So far the neural network ansatz was able to identify relatively simple states such as the Neel or stripe order. Is it capable of finding more exotic phases with complicated symmetry breaking patterns? How can it be applied to compute and classify the entanglement signatures of quantum spin liquids? Does it provide an accurate, practical method to determine the phase transitions by computing the order parameters and correlation functions? Very recently, certain limitations to the expressive power of RBMs as well as the stochastic re-configuration algorithm have been noted. For example, in some cases, the algorithm suffers from inherent numer-

ical instabilities [14, 26]. For highly frustrated quantum spin models, e.g. near  $J_2/J_1 = 0.5$  in the  $J_1$ - $J_2$  model, the energy landscape is believed to be rugged, the approach to the global minimum may not be guaranteed in practice. These limitations led to ongoing efforts to represent the amplitude and the phase of the wave function separately using two real-valued networks, and to learn the sign structures of the wave function to facilitate the convergence [14].

In light of these open issues, in this work we apply the neural network ansatz to the tripod model [27], a frustrated quantum spin model in two dimensions. It contains the Kitaev model [28] as a special limit and has an extended spin liquid phase. At the same time, its phase diagram also includes the Neel order and a non-trivial bond order which, according to TN calculations [27], can be viewed as a periodic lattice of spin vortices. Thus, this model provides an ideal playground to test the performance and limitations of the neural network ansatz. We note that previously, there have been several works that applied neural networks to study the ground state and excitations of the Kitaev model or its generalizations, e.g. with external magnetic field or Heisenberg terms [29–32]. The model here is rather different: it overlaps with the Kitaev model only at one special point. Moreover, our primary focus is on the phase diagram and phase transitions between the spin liquid and the long-range ordered states.

This paper is organized as follows. In section II, we introduce the tripod model and summarize existing numerical results from tensor network ansatz. Then we outline the RBM ansatz in section III. Section IV gives a detailed discussion of our main numerical results, including the energy, the order parameters, and the resulting phase diagram. In section V, we discuss the limitations of the neural network ansatz as implemented in our work, and directions for future improvement. We hope our results, including the strategies employed to facilitate the learning process, can be useful for applying the neural network ansatz to other quantum spin models, and more generally, to quantum many-body physics.

## II. THE TRIPOD MODEL

The tripod model is a quantum spin model defined on the two dimensional honeycomb lattice. It belongs to compass spin models, a broad class of Hamiltonians in which the exchange interaction between two neighboring spins depends on the spatial direction of the bond. The study of compass models has a long history, for review see Ref. [33]. Perhaps the best known example is the Kitaev model [28]: along the three bond directions of the honeycomb lattice, the spin exchange interaction is given by  $S_x S_x$ ,  $S_y S_y$ , and  $S_z S_z$  respectively (in this shorthand notation, the first spin operator is for one lattice site and the second for a neighboring site). Another interesting example of compass models is the quantum  $120^\circ$  model

discovered by Zhao and Liu [34], and independently by Wu [35], in the study of strongly interacting  $p$ -orbital fermions. In this model, the spin exchanges along the three bonds of the honeycomb lattice are given by  $S_1 S_1$ ,  $S_2 S_2$ , and  $S_3 S_3$  respectively. In spin space, each spin operator is represented by a vector, and here the three spin vectors  $S_{1,2,3}$  lie within a plane forming  $120^\circ$  angle with each other. It is apparent that the  $120^\circ$  model is a cousin of the Kitaev model where the three corresponding spin vectors  $S_{x,y,z}$  form an orthogonal triad in spin space (i.e.  $90^\circ$  angles with each other). This intimate connection between the two models motivated the authors of Ref. [27] to unify the  $120^\circ$  model, the Kitaev model, and the Ising model into a single compass model parameterized by an angle  $\theta$ . Its Hamiltonian is given by

$$H = J \sum_{\mathbf{r}, \gamma} S_\gamma(\mathbf{r}) S_\gamma(\mathbf{r} + \mathbf{e}_\gamma). \quad (1)$$

Here  $J > 0$  is the antiferromagnetic coupling,  $\mathbf{r}$  labels the lattice site, and  $\mathbf{e}_\gamma$  with  $\gamma = 1, 2, 3$  denotes the three bond vectors of the honeycomb lattice, i.e.  $\mathbf{r} + \mathbf{e}_\gamma$  is a neighboring site of  $\mathbf{r}$  (we have set the lattice spacing to one). The spin  $1/2$  operator  $S_\gamma$  is defined as

$$S_\gamma = \frac{1}{2}(\tau_z \cos \phi_\gamma + \tau_x \sin \phi_\gamma) \cos \theta + \frac{1}{2} \tau_y \sin \theta \quad (2)$$

where  $\tau_x, \tau_y, \tau_z$  are the Pauli matrices, and  $\phi_\gamma = 0, 2\pi/3, 4\pi/3$  are the azimuthal angle of the corresponding bond direction  $\mathbf{e}_\gamma$ . For brevity, we have suppressed the  $\theta$  dependence of  $S_\gamma$  and  $H$ , and the notation  $S_\gamma(\mathbf{r})$  means the spin operator  $S_\gamma$  is localized at site  $\mathbf{r}$ .

Model Eq. (1) is dubbed the tripod model, because geometrically the three  $S_\gamma$  form a tripod in the spin space as shown in Fig. 1 of Ref. [27]. They are tilted out of the  $xz$  plane by angle  $\theta$  and, when projected onto the  $xz$  plane, are  $120^\circ$  from each other. In addition to the tilting angle  $\theta$  that defines  $S_\gamma$ , it is convenient to follow Ref. [27] to introduce  $\theta'$ , the angle between  $S_1$  and  $S_2$ , i.e. the angle subtended by the two adjacent legs of the tripod. The two angles are related by  $\cos \theta' = 1 - (3/2) \cos^2 \theta$ . Three limits can be identified as we change  $\theta$  from  $0$  to  $90^\circ$ . At  $\theta = 0$  (and correspondingly  $\theta' = 120^\circ$ ), the three legs of the tripod  $S_{1,2,3}$  are fully open and lie within the  $xz$  plane. In this limit,  $H$  reduces to the quantum  $120^\circ$  model. As  $\theta$  is increased, the three legs are increasingly tilted out of the  $xz$  plane, corresponding to a partially open tripod. At  $\theta = \theta_K = 35.26^\circ$ ,  $\theta'$  becomes exactly  $90^\circ$ , then the tripod model becomes the Kitaev model: now that the three operators  $S_\gamma$  are orthogonal to each other, we can carry out a spin rotation and redefine them as  $S_{x,y,z}$ . Finally, when  $\theta$  is increased all the way to  $90^\circ$ , we have  $\theta' = 0$  and all three  $S_\gamma$  collapse to the  $y$  axis. The tripod is now fully closed. In this limit,  $H$  reduces to the Ising model,  $H = (J/4) \sum_{\mathbf{r}, \gamma} \tau_y(\mathbf{r}) \tau_y(\mathbf{r} + \mathbf{e}_\gamma)$ . Note that usually the Ising interaction is written in the form of  $\tau_z \tau_z$ . Here to make it easier to compare with previous literature, we follow the convention to choose  $\tau_y$

as the vertical axis in spin space [27]. This choice of the axes is particularly convenient to recover the  $120^\circ$  model defined in earlier work Ref. [34]. In passing, we note that the tripod model is not only of theoretical interest due to its synthesis of three important models in quantum magnetism. Recent experiments on honeycomb antiferromagnet  $\text{NaNi}_2\text{BiO}_{6-\delta}$  suggest that its dominant exchange interactions resemble those in the tripod model with additional terms, such as the Heisenberg exchange, also playing a role [37].

Some limits of the tripod model are easy to understand. For example, in the Ising limit, the ground state has Neel order, and the order parameter is the staggered magnetization along  $y$ . At the Kitaev point, the model is analytically solvable, and its ground state is a spin liquid and has no long-range magnetic order [28]. Aside from these two limits, for general  $\theta$ , the tripod model must be solved numerically. This is challenging because the model is frustrated and hosts highly nontrivial quantum phases. In particular, the ground state of the  $120^\circ$  model has been somewhat controversial [34–36]. It was conjectured to be long-range ordered despite the geometric frustration [35]. Ref. [27] for the first time solved the tripod model for general  $\theta'$  and obtained its ground state phase diagram using tensor network ansatz. The main conclusion is that there are three phases separated by two phase transitions, see Fig. 1 of Ref. [27]. In particular it predicted that the ground state of the  $120^\circ$  model has valence bond order. In this state, all the spin are confined within the  $xz$  plane to form a periodic pattern which can be viewed as a triangular lattice of hexagons. Around each hexagon, the spin winds successively at a  $60^\circ$  interval, forming a discrete spin vortex, see Fig. 5 of Ref. [27]. Note that this phase was referred to as “dimer phase” in Ref. [27], because along the bonds connecting these hexagons, two neighboring spins point in opposite directions. Such a terminology is unconventional, because in the literature “dimer” is usually synonymous to spin singlet. To avoid potential confusion, we prefer to call this phase having *valence bond order*, because it features spatially periodic modulations of the bond energy. TN ansatz also predicted that the quantum spin liquid is stabilized within the finite window  $\theta' \in [87^\circ, 94^\circ]$  enclosing the Kitaev point  $\theta' = 90^\circ$ . Judging from the variation of the order parameters with  $\theta'$ , the valence bond to spin liquid transition seems continuous, while the spin liquid to Neel transition seems to be first order [27].

The main goal of the present work is to investigate the ground state phase diagram of the tripod model using an independent method. This serves two purposes. On the one hand, the variational calculation with neural network ansatz here provides a check for the TN results, especially regarding the ground state in the  $120^\circ$  limit as well as the location and nature of the phase transitions. On the other hand, the calculation tests the capacity of the neural network ansatz by applying it to solve a frustrated quantum spin model which has not only spin liquid but also nontrivial long-range order with an intri-

cate spatial pattern. A priori, it is unclear whether these ground states, the order parameters, or phase transitions can be captured by the neural network ansatz. Overall, our calculation benchmarks the efficiency, stability, and accuracy of the neural network algorithm by comparing to the state-of-the-art TN results.

### III. RESTRICTED BOLTZMANN MACHINES

We will represent the many-spin wave function using one of the simplest neural networks, the Restricted Boltzmann Machines (RBMs). The implementation follows the original work of Ref. [9]. To avoid repetition, here we only outline the main ideas. More details can be found in Ref. [9] and [10]. A restricted Boltzmann machine is a shallow neural network with two layers, the visible layer consisting of  $N$  nodes characterized by spin variables  $s_i$  ( $i = 1, 2, \dots, N$ ) and a hidden layer of  $M$  nodes described by variables  $h_j$  ( $j = 1, 2, \dots, M$ ). The coupling between node  $s_i$  and node  $h_j$  is described by a connection weight  $w_{ij}$ . The quantum mechanical wave function takes the form of joint Boltzmann weight [9],

$$\begin{aligned} |\Psi\rangle &= \sum_{\{s_i\}} \psi(\mathbf{s}) |\{s_i\}\rangle \\ &= \sum_{\{s_i\}} \sum_{\{h_j\}} e^{a_i s_i + b_j h_j + w_{ij} s_i h_j} |\{s_i\}\rangle. \end{aligned} \quad (3)$$

Here, repeated indices in the exponent are summed over,  $\{s_i\} = \{s_1, s_2, \dots, s_N\}$  are all possible spin configurations (similarly for  $\{h_j\}$ ), the biases  $a_i$  and  $b_j$  as well as the connection weights  $w_{ij}$  are all complex variational parameters. Even though there is no direct intra-layer connection in a “restricted” Boltzmann machine, the hidden nodes induce correlations among the visible nodes. For real biases and connections, it is known that RBMs can represent any classical distribution to desired accuracy with sufficient numbers of hidden units [8]. The expressive power of complex RBMs is less known. It has been argued that a fully connected RBM can capture entanglement bounded by volume law and hence efficiently describe the ground states of many Hamiltonians [17]. In our calculations, we consider a finite honeycomb lattice with  $L \times L$  unit cells with periodic boundary conditions. Then the number of sites  $N = 2L^2$  and the number of bonds  $N_b = 3L^2$ . The layer density ratio  $\alpha = M/N$  is a tuning parameter, we find  $\alpha = 2$  gives satisfactory performance for  $L = 4$ .

Starting from some initial guess, e.g. random values, the variational parameters are adjusted iteratively to minimize the variation energy  $E = \langle \Psi | H | \Psi \rangle$ , the expectation value of the Hamiltonian Eq. (1) for the current wave function Eq. (3), computed approximately by Monte Carlo sampling [9]. This is done by making stochastic moves in a large parameter space based on estimating the energy gradient. This stochastic optimization procedure is often called *learning*, or training the RBM.

Here many mature algorithms from the machine learning literature can be applied [7, 38]. For example, we have tested and compared several algorithms including stochastic gradient descent, adagrad, and adamax [38–40]. The actual computation is carried out using the powerful Netket library [40], aided by custom-made routines to manipulate the variational wave functions directly.

We emphasize that while the model and learning algorithm are relatively straightforward to set up, the actual training of the RBM with a vast parameter space is by no means a trivial task. This is analogous to many other complex machine learning tasks: efficient training a neural network hinges on understanding the particularities of the model, the parameter space, and the quantity and quality of the data etc. [38, 39]. For example, starting from a random configuration of the RBM, the algorithm may lead to a quick convergence to a local minimum and stall there. This becomes especially problematic in regions where a few orders compete: for example, a blind stochastic search often yields wildly fluctuating results for two neighboring parameters that belong to the same phase. In this case, one may find the best energetics by trying different optimization algorithms or starting from different initial guesses. Even when the true ground state is being approached, the accuracy of the converged energy depends critically on the proper choice of the parameters such as learning rate and sampling batch size. A more serious problem is the sporadic occurrence of numerical instability, presumably due to the parameters being complex, which may manifest as a fast runaway of the energy toward divergence. These numerical complexities complicate the task of finding the ground state phase diagram. Some of the strategies we employ to alleviate these problems are discussed below in section IV.

#### IV. GROUND-STATE PHASE DIAGRAM

The procedure to learn the phase diagram of the tripod model is as follows. For a given value of the tilting angle  $\theta$ , the restricted Boltzmann machine is started from random parameter values, then stochastic moves are made to lower the variational energy until convergence is achieved. A crucial parameter here is the learning rate  $r$ , or step size of the stochastic moves [38, 39]. For stochastic gradient descent, choosing a  $r$  that is too large can easily end up with numerical instability, while having  $r$  too small may slow the learning to a crawl and trap it inside a local minimum. The optimal value of  $r$  depends on the model and the optimizer (many popular optimizers use adaptive learning rates determined from gradient and/or momentum). Its order of magnitude is determined by trial and error, and its value is adjusted on the fly, for example, when entering a flat energy landscape. When the algorithm fails to reach the anticipated energy, different optimizers or learning parameters are tried to shake things up. If no further progress can be made, the machine is restarted. Some states, for exam-

ple the Neel state, are rather easy to reach with fast and robust convergence. Other states, such as the spin liquid or bond order, require many more steps for the energy to relax. This is expected because of the frustration and the presence of many competing orders. To facilitate the search for ground states in highly frustrated regimes, it is useful to start from wave functions that were learned previously for parameters nearby and have competitive energies. In this case, random fluctuations are introduced to the wave function before the run, and the result must be compared to those obtained from random, blind guesses. During the run, the statistical errors (variance or standard deviation) of the observables are also monitored.

Fig. 1 shows the energy per bond in units of  $J$ ,  $\epsilon = E/N_b J$ , as a function of the tilting angle  $\theta$ . The energy is the lowest in the Ising limit  $\theta = 90^\circ$ , and the neural network ansatz accurately reproduces the analytical result  $\epsilon = -1/4$ , corresponding to the antiparallel alignment of neighboring spins. The convergence to ground state in this limit is rather fast, perhaps due to the classical nature of the Ising model. (In comparison, for  $\theta < 50^\circ$ , reaching the ground state is not as straightforward and requires some of the strategies outlined above.) As  $\theta$  is reduced,  $\epsilon$  rises quickly; and after going through the Kitaev point  $\theta_K = 35.26^\circ$ , it reaches its peak value of  $\epsilon \simeq -0.122$  at  $\theta = 34^\circ$ . The elevation in energy is in accordance with the fact that in this region around  $\theta_K$  the system is most frustrated. Upon further reduction of  $\theta$ , the energy starts to decrease. The noticeable cusp in energy located at  $\theta = 34^\circ$  marks the transition to the bond ordered phase, inside which the frustration is relieved to some degree but not entirely. This trend continues until the  $120^\circ$  model limit is reached at  $\theta = 0$ . Note the spin liquid to Neel transition is not obvious by inspecting the energy alone. But plotting  $d\epsilon/d\theta$  reveals a sudden change at  $\theta \sim 40^\circ$ . In what follows, we present a better way to reveal the phase boundaries by computing the order parameters and spin correlation functions.

The first marker of phase transition is provided by the spin-spin correlation function. It measures the antiferromagnetic long-range order and is defined by

$$C_y = \frac{4}{N-1} \sum_{j \neq i} \eta_{ij} [\langle S_y(i) S_y(j) \rangle - \langle S_y(i) \rangle \langle S_y(j) \rangle]. \quad (4)$$

Here  $i, j$  label the sites, and  $\eta_{ij} = 1$  (-1) if  $i$  and  $j$  belong to the same (different) sublattice. As shown in Fig. 2,  $C_y$  decays from 1 in the Ising limit and drops sharply as the spin liquid phase is approached. The drop experiences a glitch at  $\theta = 39^\circ$ , and  $C_y$  vanishes for  $\theta \leq 34^\circ$ . This plot clearly demonstrates the existence of Neel order at  $\theta > 39^\circ$ , as well as the lack of out-of-plane antiferromagnetic correlation for  $\theta < 34^\circ$ .

The second marker for phase transition is the expectation value of the in-plane spin

$$S_\perp = \frac{1}{N} \sum_i \sqrt{\langle S_x(i) \rangle^2 + \langle S_z(i) \rangle^2} \quad (5)$$

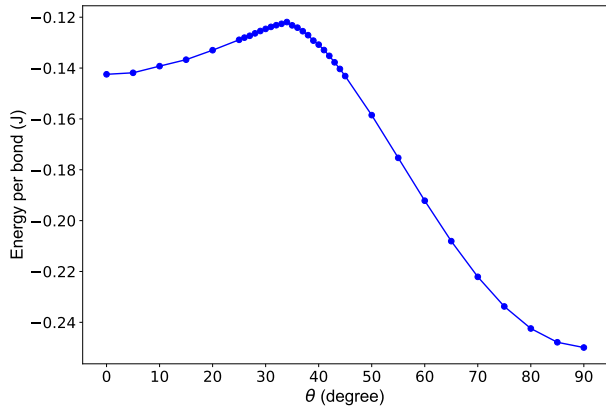


FIG. 1. The converged variational ground state energy per bond in units of  $J$  for the tripod model Eq. (1) obtained from Restricted Boltzmann Machines. Here  $\theta$  is the tilting angle out of the  $xz$  plane.  $\theta = 90^\circ$  is the Ising limit,  $\theta = 35.26^\circ$  is the Kitaev point, and  $\theta = 0^\circ$  realizes the quantum  $120^\circ$  model. The system has 64 sites with periodic boundary conditions,  $L = 4$ ,  $\alpha = 2$ . No symmetry is enforced. The statistical error is smaller than the symbol size.

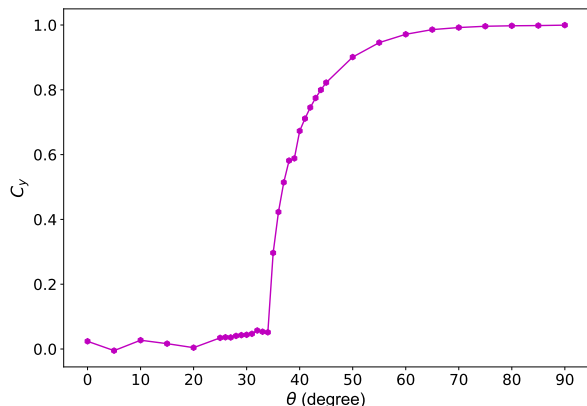


FIG. 2. The spin-spin correlation function  $C_y$  defined in Eq. (4) as function of  $\theta$ . It measures the out-of-plane antiferromagnetic order, and approaches 1 in the Ising limit. Its rapid decay to almost zero at  $\theta = 34^\circ$  and the visible kink at  $\theta = 39^\circ$  suggest two quantum phase transitions.

where  $\langle S_x(i) \rangle$  is the expectation value of local spin operator  $S_x(i)$ , and the sum  $\sum_i$  is over all sites. Fig. 3 shows the variation of  $S_\perp$  with  $\theta$ , which exhibits a trend opposite to  $C_y$ : it assumes large values within the bond ordered phase, drops sharply around  $\theta_1 \sim 34^\circ$ , followed by a small glitch at  $\theta_2 \sim 39^\circ$ . Afterwards, it remains suppressed and vanishes in the Ising limit where all the spins align parallel to the  $y$ -axis. This result confirms that the spins are predominantly in-plane within the bond ordered phase, in good agreement with TN results (see plot of  $O_2$

in Fig. 2 of Ref. [27]). Combining Fig. 2 and Fig. 3 together, it is clear that an intermediate (the spin liquid) region is bounded by the lower critical point  $\theta_B = 34^\circ$  and the upper critical point  $\theta_N = 39^\circ$ . These critical values are close to, but not identical with, the TN results  $\theta_B = 33^\circ$  and  $\theta_N = 38^\circ$  (the phase boundaries were given in Ref. [27] in terms of  $\theta'$ , which can be easily converted into  $\theta$ ).

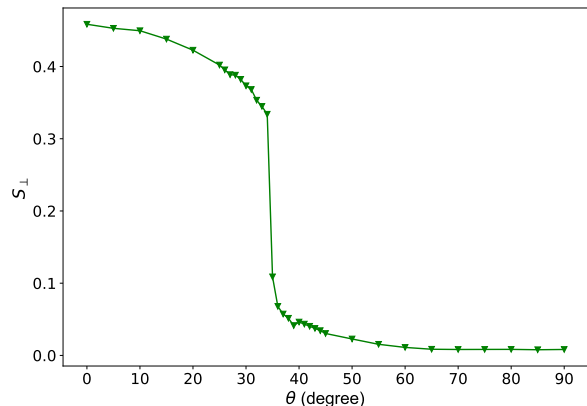


FIG. 3. The in-plane spin  $S_\perp$  defined in Eq. (5). Its maximum is achieved at  $\theta = 0$  and remains finite within the bond ordered phase. The sudden drop at  $\theta = 34^\circ$  provides a clear marker for the bond order to spin liquid transition. Transition to Neel phase is accompanied by a small bump around  $\theta \sim 40^\circ$ . Within the Neel phase,  $S_\perp$  is very small and vanishes in the Ising limit.

To further elucidate the nature of the bond ordered phase, we compute the bond energies

$$B_\gamma(\mathbf{r}) = 4\langle S_\gamma(\mathbf{r})S_\gamma(\mathbf{r} + \mathbf{e}_\gamma) \rangle \quad (6)$$

for all three bonds connected to a given site at  $\mathbf{r}$ . One then notices that for  $\theta < \theta_B$ , one of the bond is stronger than the other two, and a bond modulation pattern develops in space which breaks the underlying lattice symmetry. There are three ways to break the symmetry of the three bonds locally. For example, in symmetry-breaking pattern  $p_1$ ,  $B_1$  is stronger (negative with larger magnitude) while  $B_2$  and  $B_3$  are roughly (up to some small fluctuations) the same but weaker. The other two patterns  $p_{2,3}$  are obtained by permuting  $\gamma = 1, 2, 3$ , e.g. bond  $B_2$  is stronger in pattern  $p_2$ . Obviously, these three patterns are related to each other by  $C_3$  rotations in real space. Let us define the bond modulation  $\Delta B$  as the difference between the stronger bond and the average of the two weaker bonds, for example,

$$\Delta B = \frac{1}{N} \sum_{\mathbf{r}} \frac{1}{2} [B_2(\mathbf{r}) + B_3(\mathbf{r})] - B_1(\mathbf{r}), \quad (7)$$

where the average over all sites is taken. A finite  $\Delta B$  is expected if the bond modulation pattern  $p_1$  is repeated

throughout the lattice. As shown in Fig. 4, the bond ordered phase is characterized by a finite bond modulation, whereas in both the Neel and spin liquid phase, bond energies are approximately uniform in space. Thus, the bond ordered phase found here has a solid order of periodically modulated bonds, i.e. a valence bond solid. It breaks the  $C_3$  symmetry of the underlying honeycomb lattice, but differs from the spin vortex state discussed in Ref. [27]. And its energy per bond  $\epsilon = -0.143$  is higher than the best TN result  $-0.148$  [27]. The reason behind this difference is addressed in the next section.

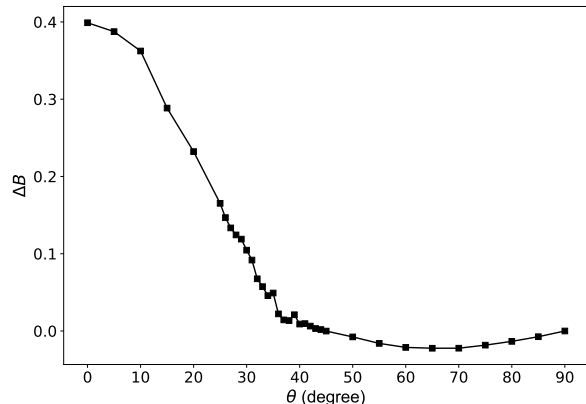


FIG. 4. Bond modulation  $\Delta B$  defined by Eq. (7) and (6). The bond ordered phase features bond modulations that grow with decreasing  $\theta$ . The Neel phase only has small fluctuations in bond energy.

## V. LIMITATIONS AND OUTLOOK

To summarize, neural network quantum states based on RBM have performed very well to identify the main phases (Neel, bond order, and spin liquid) and phase transitions of the frustrated tripod model. We find it remarkable that with some judicious control over the learning parameters and learning strategy, the algorithm can efficiently navigate the  $2^{64}$ -dimensional Hilbert space stochastically to find variational ground states that have competitive energies and capture the essential physics. In particular the two phase boundaries are close to the state-of-the-art TN ansatz. And for smaller systems, e.g.  $L = 3$ , the energetics is also in excellent agreement with exact diagonalization.

Our study also exposes some of the limitations of the neural network ansatz as implemented here. The most obvious weakness is the lack of symmetry constraints in our calculation: we did not pose any symmetry on the wave functions (or more specifically on the RBM parameters). While this has the advantage of being completely unbiased, it also makes it exceedingly hard, if not at all impossible, to reach intricate states such as the spin vor-

text lattice proposed in Ref. [27] for the  $120^\circ$  model. In Fig. 4 above, our calculation reaches one of the periodic bond modulation patterns, i.e. the repetition of local pattern  $p_1$ . There are two other states, where pattern  $p_2$  or  $p_3$  is repeated instead, with degenerate energies. Moreover, any covering of the lattice with some combination of pattern  $p_{1,2,3}$  has the same classical energy, giving rise to a large residue entropy similar to spin ice [41]. The quantum Hamiltonian Eq. (1) induces transitions between different coverings and lifts the classical degeneracy, then a particular covering, or superpositions of different coverings, may acquire lower energy to become the quantum mechanical ground state. For example, the vortex state of Ref. [27] represents a particular periodic covering of the whole lattice with local bond pattern  $p_1$ ,  $p_2$ , and  $p_3$ . We conjecture this state may be eventually reached by RBM with further refinement in energy. In practice, this turns out to be hard, because of the flatness of the energy landscape (different covering patterns have close energies) and the diminishing probability of settling into a configuration with a large unit cell and high symmetry by pure stochastic moves in a huge parameter space. Our attempts to improve the energy, for example by perturbing the wave function, frequently lead to numerical instabilities. Presumably, this barrier can be overcome by applying symmetry constraints [11, 42, 43], e.g. by enforcing  $C_6$  symmetry or fixing the unit cell shape and size and then comparing converged states with different symmetries or unit cells.

Fig. 4. shows another caveat of unconstrained learning in large systems: there are small but visible fluctuations in the bond energy even in the Neel phase. Even though the algorithm successfully approaches the antiferromagnetic ground state with excellent energy, in practice we find the RBM rarely settles into a completely frozen state. The stochastic nature of the algorithm unavoidably introduces low lying excitations, which for larger systems (with significantly more parameters to vary) are increasingly harder to eliminate. This creates a dilemma: on the one hand we need large clusters to accommodate orders with long modulation periods, on the other hand for large systems it usually becomes more challenging to relax to pristine long-range ordered states.

Given these considerations, we advocate the following strategy to make the best out of the neural network ansatz. First, the unconstrained network is trained to find the rough phase diagram and symmetry breaking patterns. It has the virtue of being unbiased. Then, other methods, such as analytical variational wave functions or neural network with symmetry, are used to further improve the energetics and elucidate the long-range order. We envision such a hybrid approach especially useful in understanding complex spin systems, for example models inspired by a large class of Kitaev materials [44, 45]. Our results suggest that, with further refinements and complemented by other approaches, variational ansatz based on neural network quantum states can serve as a powerful tool to understand frustrated quantum spin models and

more generally strongly interacting many-body systems.

### ACKNOWLEDGMENTS

This work is supported by NSF Grant No. PHY-2011386 (EZ). EZ would like to thank Christian McGuirk

for preliminary work implementing and benchmarking RBM and Mahmoud Lababidi, Ahmet Keles and Haiyuan Zou for illuminating discussions. The numerical simulation is based on the Netket library version 2.1.1 [40]. Part of the calculation was carried out on the ARGO clusters provided by the Office of Research Computing at George Mason University.

- 
- [1] C. Lacroix, P. Mendels, F. Mila, eds. Introduction to frustrated magnetism: materials, experiments, theory. Springer, 2011.
- [2] H. T. Diep, ed. Frustrated spin systems. World Scientific, 2013.
- [3] L. Savary, L. Balents. Quantum spin liquids: a review. *Reports on Progress in Physics* 80, 016502, 2016.
- [4] F. Verstraete and J. I. Cirac, Renormalization algorithms for quantum-many body systems in two and higher dimensions. *arXiv:cond-mat/0407066*, 2004.
- [5] R. Orus, A practical introduction to tensor networks: Matrix product states and projected entangled pair states. *Annals of Physics* 349, 117, 2014.
- [6] F. Verstraete, V. Murg, J. I. Cirac. Matrix product states, projected entangled pair states, and variational renormalization group methods for quantum spin systems. *Advances in Physics* 57, 143, 2008.
- [7] P. Mehta, M. Bukov, C.-H. Wang, A. G. Day, C. Richardson, C. K. Fisher, and D. J. Schwab. A high-bias, low-variance introduction to machine learning for physicists. *Physics Reports* 810, 1, 2019.
- [8] N. Le Roux and Y. Bengio. Representational power of restricted Boltzmann machines and deep belief networks. *Neural Computation* 20, 1631, 2008.
- [9] G. Carleo and M. Troyer. Solving the quantum many-body problem with artificial neural networks. *Science* 355, 602, 2017.
- [10] R. G. Melko, G. Carleo, J. Carrasquilla, and J. I. Cirac. Restricted Boltzmann machines in quantum physics. *Nature Physics* 15, 887, 2019.
- [11] K. Choo, T. Neupert, and G. Carleo. Two-dimensional frustrated J1-J2 model studied with neural network quantum states. *Physical Review B* 100, 125124, 2019.
- [12] X. Liang, W.-Y. Liu, P.-Z. Lin, G.-C. Guo, Y.-S. Zhang, L. He. Solving frustrated quantum many-particle models with convolutional neural networks. *Physical Review B* 98, 104426, 2018.
- [13] Z. Cai and J. Liu. Approximating quantum many-body wave functions using artificial neural networks. *Physical Review B* 97, 035116, 2018.
- [14] M. Bukov, M. Schmitt, M. Dupont. Learning the ground state of a non-stoquastic quantum Hamiltonian in a rugged neural network landscape. *SciPost Physics* 10, 147, 2021.
- [15] Y. Nomura and M. Imada. Dirac-type nodal spin liquid revealed by refined quantum many-body solver using neural-network wave function, correlation ratio, and level spectroscopy. *Physical Review X* 11, 031034, 2021.
- [16] D. Kochkov, T. Pfaff, A. Sanchez-Gonzalez, P. Battaglia, and B. K. Clark. Learning ground states of quantum Hamiltonians with graph networks. *arXiv:2110.06390* (2021).
- [17] J. Chen, S. Cheng, H. Xie, L. Wang, and T. Xiang. Equivalence of restricted Boltzmann machines and tensor network states. *Physical Review B* 97, 085104, 2018.
- [18] I. Glasser, N. Pancotti, M. August, I. D. Rodriguez, and J. I. Cirac. Neural-Network Quantum States, String-Bond States, and Chiral Topological States. *Physical Review X* 8, 011006, 2018.
- [19] Y. Huang and J. E. Moore. Neural Network Representation of Tensor Network and Chiral States. *Physical Review Letters* 127, 170601, 2021.
- [20] D.-L. Deng, X. Li, and S. Das Sarma. Quantum Entanglement in Neural Network States. *Physical Review X* 7, 021021, 2017.
- [21] D.-L. Deng, X. Li, and S. Das Sarma. Machine learning topological states. *Physical Review B* 96, 195145, 2017.
- [22] R. Kaubruegger, L. Pastori, and J. C. Budich. Chiral topological phases from artificial neural networks. *Physical Review B* 97, 195136, 2018.
- [23] Y. Nomura, A. S. Darmawan, Y. Yamaji, and M. Imada. Restricted Boltzmann machine learning for solving strongly correlated quantum systems. *Physical Review B* 96, 205152, 2017.
- [24] P. Broecker, J. Carrasquilla, R. G. Melko, and S. Trebst. Machine learning quantum phases of matter beyond the fermion sign problem. *Scientific Reports* 7, 8823, 2017.
- [25] K. Ch'ng, J. Carrasquilla, R. G. Melko, and E. Khatami. Machine learning phases of strongly correlated fermions. *Physical Review X* 7, 031038, 2017.
- [26] C. Y Park, M. J. Kastoryano. Are neural quantum states good at solving non-stoquastic spin Hamiltonians? *arXiv:2012.08889*, 2020.
- [27] H. Zou, B. Liu, E. Zhao, W. V. Liu. A continuum of compass spin models on the honeycomb lattice. *New Journal of Physics* 18, 053040, 2016.
- [28] A. Kitaev. Anyons in an exactly solved model and beyond. *Annals of Physics* 321, 2, 2006.
- [29] M. Noormandipour, Y. Sun, B. Haghghat, Restricted Boltzmann machine representation for the ground state and excited states of Kitaev honeycomb model, *arXiv:2003.07280*, 2020.
- [30] D. A. Puente, I. M. Eremin. Convolutional restricted Boltzmann machine aided Monte Carlo: An application to Ising and Kitaev models. *Physical Review B* 102, 195148, 2020.
- [31] C.-X. Li, S. Yang, J.-B. Xu, Learning spin liquids on a honeycomb lattice with artificial neural networks, *Scientific Reports* 11, 16667 (2021)
- [32] N. Rao, K. Liu, M. Machaczek, L. Pollet. Machine-learned phase diagrams of generalized Kitaev honeycomb magnets. *Physical Review Research* 3, 033223, 2021
- [33] Z. Nussinov and J. van den Brink. Compass models: Theory and physical motivations. *Review of Modern Physics*

- 87, 1, 2015.
- [34] E. Zhao and W. V. Liu. Orbital order in Mott insulators of spinless p-band fermions. *Physical Review Letters* 100, 160403, 2008.
- [35] C. Wu. Orbital Ordering and Frustration of p-Band Mott Insulators. *Physical Review Letters* 100, 200406, 2008.
- [36] J. Nasu, A. Nagano, M. Naka, S. Ishihara. Doubly degenerate orbital system in honeycomb lattice: Implication of orbital state in layered Iron oxide. *Physical Review B* 78, 024416 (2008).
- [37] A. Scheie, K. Ross, P. P. Stavropoulos, E. Seibel, J. A. Rodriguez-Rivera, J. A. Tang, Yi Li, H.-Y. Kee, R. J. Cava, C. Broholm, Counterrotating magnetic order in the honeycomb layers of  $\text{NaNi}_2\text{BiO}_{6-\delta}$ . *Physical Review B* 100, 214421, 2019
- [38] I. Goodfellow, Y. Bengio, A. Courville. Deep learning. MIT press, 2016.
- [39] A. Geron. Hands-On Machine Learning with Scikit-Learn, Keras, and TensorFlow: Concepts, Tools, and Techniques to Build Intelligent Systems. 2nd Edition, O'Reilly Media, 2019.
- [40] G. Carleo, K. Choo, D. Hofmann, J. E. T. Smith, T. Westerhout, F. Alet, E. J. Davis, S. Efthymiou, I. Glasser, S.-H. Lin, M. Mauri, G. Mazzola, C. B. Mendl, E. van Nieuwenburg, O. O'Reilly, H. Theveniaut, G. Torlai, A. Wietek. NetKet: A machine learning toolkit for many-body quantum systems. *Software X* 10, 100311, 2019.
- [41] A. P. Ramirez, A. Hayashi, R. J. Cava, R. Siddharthan, B. S. Shastry. Zero-point entropy in 'spin ice'. *Nature* 399, 333, 1999.
- [42] Y. Nomura. Helping restricted Boltzmann machines with quantum-state representation by restoring symmetry. *Journal of Physics: Condensed Matter* 33, 174003, 2021.
- [43] C. Roth and A. H. MacDonald. Group convolutional neural networks improve quantum state accuracy. *arXiv:2104.05085*, 2021.
- [44] S. M. Winter, Y. Li, YH. O. Jeschke, R. Valenti. Challenges in design of Kitaev materials: Magnetic interactions from competing energy scales. *Physical Review B* 93, 214431, 2016.
- [45] S. Trebst. Kitaev materials. *arXiv:1701.07056*, 2017.